


RESEARCH ARTICLE

Open Access



# A comparison of 2D and 3D magnetic resonance imaging-based intratumoral and peritumoral radiomics models for the prognostic prediction of endometrial cancer: a pilot study

Ruixin Yan<sup>1</sup>, Siyuan Qin<sup>1</sup>, Jijia Xu<sup>1</sup>, Weili Zhao<sup>1</sup>, Peijin Xin<sup>1</sup>, Xiaoying Xing<sup>1</sup> and Ning Lang<sup>1\*</sup> 

## Abstract

**Background** Accurate prognostic assessment is vital for the personalized treatment of endometrial cancer (EC). Although radiomics models have demonstrated prognostic potential in EC, the impact of region of interest (ROI) delineation strategies and the clinical significance of peritumoral features remain uncertain. Our study thereby aimed to explore the predictive performance of varying radiomics models for the prediction of LVSI, DMI, and disease stage in EC.

**Methods** Patients with 174 histopathology-confirmed EC were retrospectively reviewed. ROIs were manually delineated using the 2D and 3D approach on T2-weighted MRI images. Six radiomics models involving intratumoral ( $2D_{intra}$  and  $3D_{intra}$ ), peritumoral ( $2D_{peri}$  and  $3D_{peri}$ ), and combined models ( $2D_{intra+peri}$  and  $3D_{intra+peri}$ ) were developed. Models were constructed using the logistic regression method with five-fold cross-validation. Area under the receiver operating characteristic curve (AUC) was assessed, and was compared using the Delong's test.

**Results** No significant differences in AUC were observed between the  $2D_{intra}$  and  $3D_{intra}$  models, or the  $2D_{peri}$  and  $3D_{peri}$  models in all prediction tasks ( $P > 0.05$ ). Significant difference was observed between the  $3D_{intra}$  and  $3D_{peri}$  models for LVSI (0.738 vs. 0.805) and DMI prediction (0.719 vs. 0.804). The  $3D_{intra+peri}$  models demonstrated significantly better predictive performance in all 3 prediction tasks compared to the  $3D_{intra}$  model in both the training and validation cohorts ( $P < 0.05$ ).

**Conclusions** Comparable predictive performance was observed between the 2D and 3D models. Combined models significantly improved predictive performance, especially with 3D delineation, suggesting that intra- and peritumoral features can provide complementary information for comprehensive prognostication of EC.

**Keywords** Magnetic resonance imaging, Endometrial cancer, Radiomics, Prognostic analysis

\*Correspondence:

Ning Lang  
langning800129@126.com

<sup>1</sup>Department of Radiology, Peking University Third Hospital, 49 North Garden Road, Haidian District, Beijing 100191, People's Republic of China



© The Author(s) 2024. **Open Access** This article is licensed under a Creative Commons Attribution 4.0 International License, which permits use, sharing, adaptation, distribution and reproduction in any medium or format, as long as you give appropriate credit to the original author(s) and the source, provide a link to the Creative Commons licence, and indicate if changes were made. The images or other third party material in this article are included in the article's Creative Commons licence, unless indicated otherwise in a credit line to the material. If material is not included in the article's Creative Commons licence and your intended use is not permitted by statutory regulation or exceeds the permitted use, you will need to obtain permission directly from the copyright holder. To view a copy of this licence, visit <http://creativecommons.org/licenses/by/4.0/>. The Creative Commons Public Domain Dedication waiver (<http://creativecommons.org/publicdomain/zero/1.0/>) applies to the data made available in this article, unless otherwise stated in a credit line to the data.

## Background

Endometrial cancer (EC) is the most common gynecological malignancy in developed country and second most common in China. Its incidence and mortality rate were still rising in recent years [1, 2]. Approximately 3% of women will develop EC in their lifetime with a median age of 61 years at first diagnosis [3]. While EC has an encouraging overall 5-year survival rate of 81% [4], clinicians face significant challenges in treatment decisions of overtreatment for low-risk patients and undertreatment for high-risk patients. Accurate risk assessment rely heavily on important histopathological factors such as International Federation of Gynecology and Obstetrics (FIGO) stage, lymphovascular space invasion (LVSI), and depth of myometrial invasion (DMI) [5–8]. While precisely determining these prognostic metrics continues to be crucial for distant relapse assessment and of poor prognosis estimation. However, such prognostic biomarkers can only be confirmed by histopathology, and is the main challenge of current clinical practice.

Magnetic resonance imaging (MRI) is considered mainstay for the preoperative evaluation of EC, given its high soft tissue contrast resolution allowing for the delineation of tumor invasion [1, 9]. However, the subjective nature in visual interpretation remains a limitation of conventional MRI. As reported by Arnaiz et al. assessing its role in disease staging, accurate prediction was only achieved in 47.2% of cases [10]. Radiomics represent a novel technique enabling the extraction of large amounts of data from medical images in a high-throughput and quantitative manner [11]. Since its advent, it has demonstrated great potential as a diagnostic and prognostic tool for a wide range of cancers [12–15]. In the context of EC, radiomics have demonstrated the value in not only the characterization of tumors, but also the prediction of high-risk diseases and survival outcomes [16–20].

Region of interest (ROI) delineation strategies can influence feature extraction and hence, affect the downstream performance of a radiomics model. Two approaches currently exist — the two-dimensional (2D) approach, which involves the delineation of lesions from a single image layer at the largest cross-section, or simply the center slice, and the three-dimensional (3D) approach, which involves the use of all tumor-containing slices. While the latter approach has been widely advocated for its comprehensiveness in tumor characterization [17, 20, 21], the need for manual delineation renders it more time-consuming and labor-intensive. As of now, the optimal ROI delineation strategy for the radiomics profiling of EC remains unclear. Besides, the majority of previous MRI-based radiomics research has placed focused on the characterization of intratumoral regions [16, 20, 21]. However, the surrounding microenvironment has

been increasingly shown to offer insight into the clinical behavior of primary lesions [22–24].

This study thereby aimed to compare the clinical value of 2D and 3D MRI-based radiomics features for the prediction of LVSI, DMI, and disease stage in EC, as well as contribute to the existing literature on the significance of peritumoral radiomics features for prognostication of the disease.

## Methods

### Patient selection

Patients diagnosed with endometrial cancer between January 2017 and December 2022 at Peking University Third Hospital were retrospectively reviewed. All patients who underwent pelvic magnetic resonance imaging (MRI) within 14 days prior to hysterectomy were considered. The exclusion criteria included the following: (1) tumors with a maximum diameter of <1 cm, (2) inadequate or poor image quality, (3) absence of relevant clinical or pathological information, (4) prior treatment with adjuvant chemotherapy or radiotherapy, and (5) non-endometrial primary malignancies.

This study was approved by the Ethics Committee of the institute (M2023637), who waived the requirement for informed patient consent.

### Clinicopathological data collection

Clinicopathological characteristics including age, DMI, LVSI, tumor stage, histopathological type and serum CA125 and CA199 levels were obtained from medical records. Histopathological assessment was performed on all surgical specimens. Tumor staging was performed according to the 2009 FIGO staging system, with stages I – II and III – IV were classified as early- and late-stage EC, respectively [25].

### Image acquisition and segmentation

Preoperative pelvic MRI was performed using 1.5 T Avanto scanner and 3.0 T Skyra scanners, with protocol parameters detailed in Supplementary Table S1. Axial T2-weighted images were acquired and used for subsequent analysis due to their ability to effectively distinguish between tumor-tissue and normal surrounding myometrial-tissue [1]. All images were imported into uAI Research Portal (V1.1, United Imaging Intelligence, Co., Ltd., Shanghai, China).

Intratumoral ROIs ( $ROI_{intra}$ ) were manually delineated by a radiologist (R.Y.) with 5-year experience, which were then reviewed and refined where necessary by a second radiologist (X.X.) with 15-year experience. Both radiologists were blinded to the study.  $ROI_{intra}$  was defined as the entire tumor volume across all tumor slices on 3D images, and as the maximum tumor cross-section on 2D images. Any cystic or hemorrhagic areas were avoided.

Peritumoral ROIs ( $ROI_{peri}$ ) were automatically delineated by extending the tumor margin by 3 mm generated using the boundary “dilation” tool in the uAI platform [19, 24].

**Image preprocessing and radiomics feature extraction**

Image preprocessing and radiomics feature extraction were performed in accordance to the Image Biomarker Standardisation Initiative (IBSI [26]). All T2-weighted images were resampled to an isotropic pixel size of  $1 \times 1 \times 1$  mm using BSpline interpolation to eliminate resolution discrepancies between devices. Pixel intensities were subsequently standardized to a common scale to further minimize background noise.

Radiomics features were extracted using the PyRadiomics python package. A total of 1197 radiomics features were extracted for each ROI, and consisted of the following 7 classes: first-order statistics (19.5%), shape-based features (1.2%), texture-based features including gray level co-occurrence matrix (GLCM) (23.9%) capturing texture, gray level run length matrix (GLRLM) (17.4%) describing gray level runs, gray level size zone matrix (GLSZM) (17.4%) characterizing zone sizes, neighboring gray tone difference matrix (NGTDM) (5.4%) quantifying differences between tumor and neighborhood pixels, and gray level dependence matrix (GLDM) (15.2%) analyzing dependency of gray levels. Subsequently Combined feature ( $ROI_{intra+peri}$ ) was fused by merging the extracted features from intra-tumoral models and respective peritumoral models. All extracted features were standardized using the Z-score normalization method to standardize the different measurement units across features, preventing model results from being influenced by feature-scale variations.

**Radiomic feature selection and machine learning model construction**

First, features with correlation coefficients  $P$ -value less than 0.05 were remained. Least absolute shrinkage and selection operator regression (LASSO) was subsequently performed to select for those with non-zero coefficients. Five-fold cross-validation was applied, features appeared in more than two times were finally selected by “vote” function on the uAI platform to establish the radiomic models.

The models were eventually constructed using selected radiomics features using logistic regression. Patients were randomly divided into five equal size subsets, one subset served as the validation set. The remaining four-fifths were the training set. This process was then repeated five times with different subsets for validation and training. The performance was averaged across the five times process to obtain a robust estimate of generalizability. The radiomics workflow is illustrated in Fig. 1.

**Statistical analysis**

All statistical analyses were conducted using the SPSS software (IBM, Chicago, IL, USA, R23.0.0.0). Diagnostic performance was assessed using the receiver operating characteristic (ROC) curve analysis in terms of areas under the ROC curve (AUC), sensitivity, and specificity and accuracy. AUCs were compared using the Delong test. and are illustrated in the form of heatmaps.

**Results**

**Baseline clinicopathological characteristics**

A total of 174 patients with EC were enrolled in our study. The patient selection process is illustrated in Fig. 2. The average age was  $56.96 \pm 11.43$  years (range, 27–86 years). Among them, 37 (21.3%) presented with late-stage

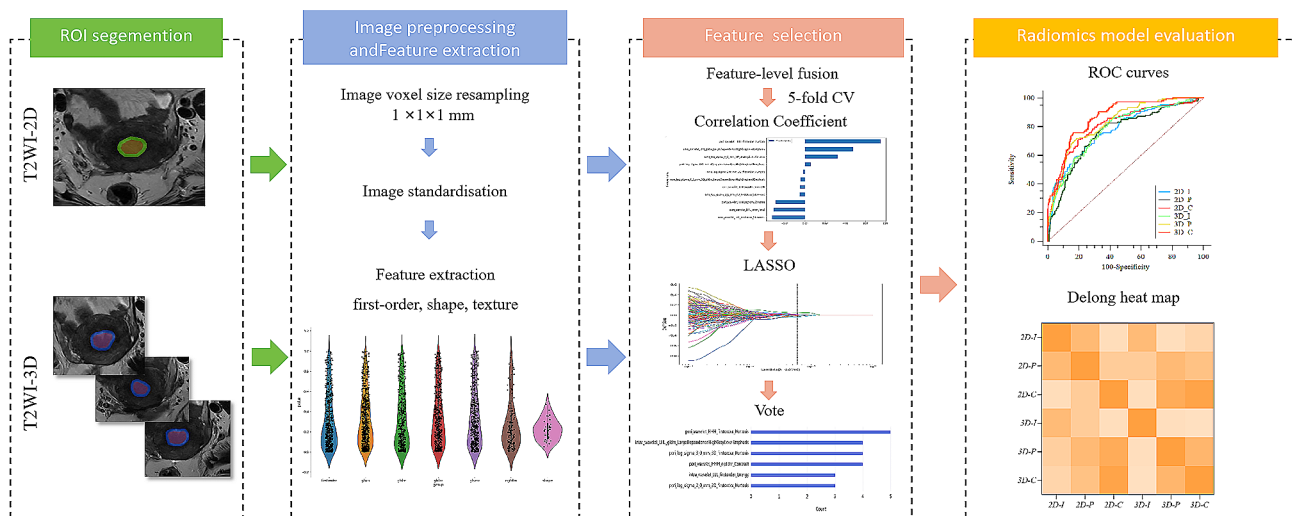


**Fig. 1** The radiomics workflow

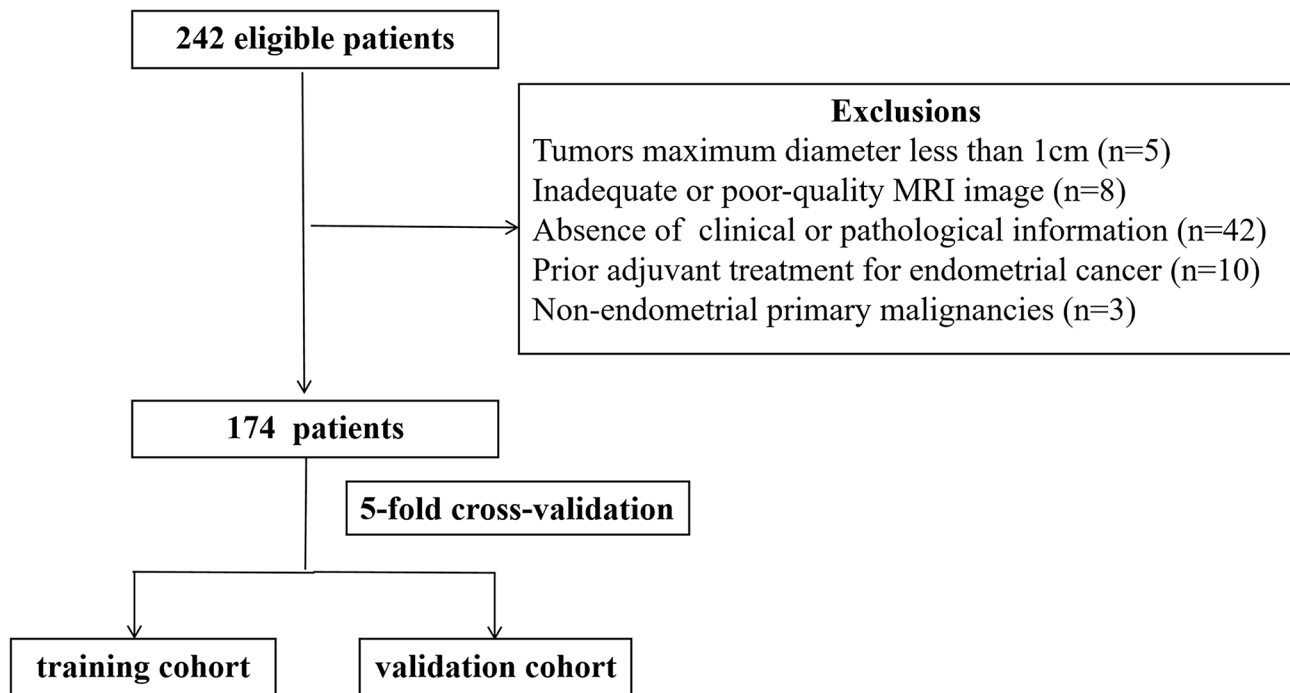


**Fig. 2** The patient selection process

**Table 1** Baseline clinicopathological characteristics of the included patients

Variables	
Age (year), $\pm$ SD	56.96 $\pm$ 11.43
FIGO stage, n (%)	
Early-stage	137 (78.7%)
Late-stage	37 (21.3%)
LVSI, n (%)	
+	39 (22.4%)
-	135 (77.6%)
DMI, n (%)	
+	55 (31.6%)
-	119 (68.4%)
CA125 (u/ml), $\pm$ SD	34.97 $\pm$ 45.70
CA199 (u/ml), $\pm$ SD	40.60 $\pm$ 88.96
Type, n (%)	
Endometrioid carcinoma	154 (88.5%)
Non-Endometrioid carcinoma	20 (11.5%)

Abbreviations: FIGO stage, International Federation of Gynecology and Obstetrics (2009) stage, stages I–II and III–IV defined as early- and late-stage EC, respectively; LVSI, lymphovascular space invasion; and DMI, deep myometrial invasion; Non-Endometrioid carcinoma: include Serous carcinoma, Clear cell carcinoma, Mixed carcinoma, Undifferentiated carcinoma and Dedifferentiated carcinoma

disease. LVSI was observed in 39 (22.4%) patients, while DMI was seen in 55 (31.6%). The most common EC cell type was observed to be endometrioid adenocarcinoma (88.5%). All baseline characteristics of the patients are shown in Table 1.

#### Radiomics feature selection

Six models,  $2D_{intra}$ ,  $2D_{peri}$ ,  $2D_{intra+peri}$ ,  $3D_{intra}$ ,  $3D_{peri}$ , and  $3D_{intra+peri}$  were constructed for each task. The total number of radiomics features retained in each model were as follows: 11, 8, 11, 2, 7, and 6, respectively, for LVSI prediction; 8, 14, 13, 14, 10, and 13, respectively, for DMI prediction; and 6, 6, 7, 7, 7, and 11, respectively, for FIGO stage prediction. The distribution of radiomics feature classes of intra- and peri-tumoral region across all models is shown in Fig. 3a. The number of intra- and peritumoral features incorporated into each model is shown in Fig. 3b. The exact feature names and type are provided in Supplementary Tables S2 – S4.

#### Predictive performance of the independent radiomics models

The ROC curve results of the six established models are shown in both Table 2; Fig. 4. The Delong test results are shown in Fig. 5 and Supplementary Tables S5 – S10.

In terms of ROI delineation strategies, significant differences were observed between the  $2D_{intra}$  and  $3D_{intra}$  models for LVSI prediction in the training cohort [0.810 (0.718–0.903) vs. 0.738 (0.634–0.844),  $P=0.001$ ]. Additionally, significant differences were shown between the  $2D_{peri}$  and  $3D_{peri}$  models for both DMI [0.928 (0.889–0.972) vs. 0.833 (0.761–0.909),  $P=0.000$ ] and stage prediction [0.760 (0.658–0.860) vs. 0.824 (0.747–0.908),  $P=0.000$ ] in the training data. Such significant differences were not observed between all models in the validation cohort ( $P>0.05$ ).

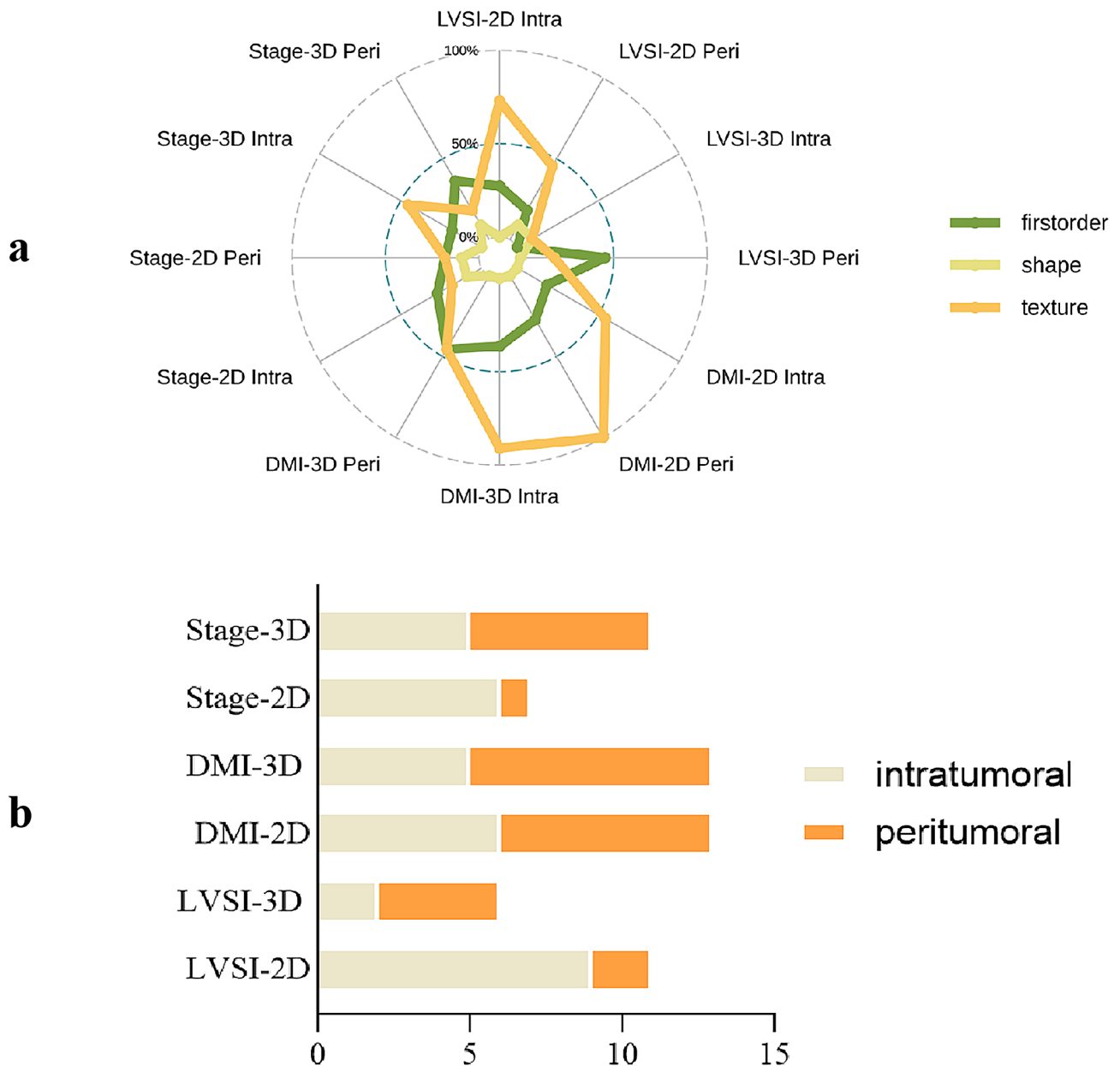


**Fig. 3** Distribution and composition of (a) the three feature classes (first-order, shape, texture) across the models, and (b) the intra- and peritumoral features across the models

In terms of intra- and peri-tumoral features, significant differences were observed between the 2D<sub>intra</sub> and 2D<sub>peri</sub> models for DMI prediction [0.784 (0.699–0.871) vs. 0.928 (0.889–0.972),  $P=0.000$ ] in the training cohort, which was not observed in the validation cohort ( $P>0.05$ ). Significant differences were observed between the 3D<sub>intra</sub> versus 3D<sub>peri</sub> models for LVSI [0.738 (0.634–0.844) vs. 0.813 (0.782–0.898),  $P=0.000$ ], DMI [0.761 (0.679–0.847) vs. 0.833 (0.761–0.909),  $P=0.000$ ], and stage prediction [0.782 (0.688–0.877) vs. 0.824 (0.747–0.908),  $P=0.049$ ] in the training cohort. Such significance remained in the validation cohort for LVSI prediction [0.738

(0.634–0.844) vs. 0.805 (0.625–0.977),  $P=0.049$ ] and DMI prediction [0.719 (0.538–0.904) vs. 0.804 (0.654–0.953),  $P=0.019$ ], but not for stage prediction [0.738 (0.540–0.932) vs. 0.763 (0.581–0.942)].

**Predictive performance of the combined radiomics models**

For LVSI prediction, the 2D<sub>intra+peri</sub> and 3D<sub>intra+peri</sub> models demonstrated AUC values of 0.853 (0.773–0.933) and 0.816 (0.730–0.901), respectively, in the training cohort and values of 0.720 (0.493–0.944) and 0.812 (0.633–0.979), respectively, in the validation cohort. For DMI prediction, the AUC values were 0.839 (0.768–0.913)

**Table 2** Logistic regression with five-fold cross-validation for predictive performance of the models

Model		Group	Mean AUC (95%CI)	ACC	SEN	SPE
LVSI	2D <sub>intra</sub>	Train	0.810 (0.718–0.903)	0.730	0.737	0.728
		Val	0.725 (0.505–0.937)	0.666	0.639	0.674
	2D <sub>peri</sub>	Train	0.784 (0.695–0.874)	0.682	0.731	0.669
		Val	0.706 (0.490–0.920)	0.644	0.668	0.637
	2D <sub>intra+peri</sub>	Train	0.853 (0.773–0.933)	0.730	0.789	0.713
		Val	0.720 (0.493–0.944)	0.667	0.639	0.674
	3D <sub>intra</sub>	Train	0.738 (0.634–0.844)	0.675	0.647	0.683
		Val	0.738 (0.534–0.933)	0.684	0.614	0.704
	3D <sub>peri</sub>	Train	0.813 (0.782–0.898)	0.726	0.769	0.713
		Val	0.805 (0.625–0.977)	0.695	0.771	0.674
	3D <sub>intra+peri</sub>	Train	0.816 (0.730–0.901)	0.737	0.750	0.733
		Val	0.812 (0.633–0.979)	0.737	0.743	0.726
DMI	2D <sub>intra</sub>	Train	0.784 (0.699–0.871)	0.762	0.636	0.819
		Val	0.760 (0.582–0.938)	0.736	0.600	0.800
	2D <sub>peri</sub>	Train	0.928 (0.889–0.972)	0.826	0.936	0.775
		Val	0.773 (0.614–0.932)	0.684	0.727	0.663
	2D <sub>intra+peri</sub>	Train	0.839 (0.768–0.913)	0.783	0.741	0.803
		Val	0.799 (0.638–0.963)	0.753	0.691	0.782
	3D <sub>intra</sub>	Train	0.761 (0.679–0.847)	0.700	0.641	0.727
		Val	0.719 (0.538–0.904)	0.679	0.618	0.707
	3D <sub>peri</sub>	Train	0.833 (0.761–0.909)	0.757	0.791	0.742
		Val	0.804 (0.654–0.953)	0.724	0.745	0.715
	3D <sub>intra+peri</sub>	Train	0.845 (0.776–0.917)	0.779	0.782	0.777
		Val	0.807 (0.653–0.959)	0.770	0.745	0.782
Stage	2D <sub>intra</sub>	Train	0.773 (0.673–0.872)	0.703	0.703	0.703
		Val	0.704 (0.478–0.928)	0.625	0.701	0.683
	2D <sub>peri</sub>	Train	0.760 (0.658–0.860)	0.716	0.699	0.703
		Val	0.706 (0.491–0.919)	0.704	0.701	0.701
	2D <sub>intra+peri</sub>	Train	0.814 (0.719–0.909)	0.757	0.725	0.731
		Val	0.687 (0.472–0.896)	0.575	0.693	0.667
	3D <sub>intra</sub>	Train	0.782 (0.688–0.877)	0.663	0.732	0.717
		Val	0.738 (0.540–0.932)	0.621	0.694	0.678
	3D <sub>peri</sub>	Train	0.824 (0.747–0.908)	0.730	0.748	0.744
		Val	0.763 (0.581–0.942)	0.704	0.715	0.713
	3D <sub>intra+peri</sub>	Train	0.864 (0.795–0.933)	0.717	0.854	0.825
		Val	0.804 (0.640–0.967)	0.700	0.833	0.805

Abbreviations: AUC, area under the receiver operating characteristic curve; ACC, accuracy; SEN: sensitivity, and SPE: specificity

and 0.845 (0.776–0.917), respectively, in the training cohort, and were 0.799 (0.638–0.963) and 0.807 (0.653–0.959), respectively, in the validation cohort. For stage prediction, significant differences were demonstrated in both the training cohort [0.814 (0.719–0.909) vs. [0.864 (0.795–0.933),  $P=0.006$ ] and the validation cohort [0.687 (95% CI, 0.472–0.896) vs. 0.804 (0.640–0.967),  $P=0.023$ ] in the validation cohort.

Compared to the 2D<sub>intra</sub> model, significantly increase in predictive performance was observed with inclusion of peritumoral features for LVSI (+0.043,  $P=0.006$ ) and DMI (+0.055, ( $P=0.000$ )) in the training cohort. Significant increase was observed for DMI prediction (+0.039,  $P=0.045$ ) in the validation cohort. Compared to the 3D<sub>intra</sub> model, significant increase in prediction efficacy

was observed for LVSI prediction (+0.078,  $P=0.000$ ), DMI prediction (+0.084,  $P=0.000$ ), and FIGO stage prediction (+0.066,  $P=0.000$ ) in the training cohort. Such significance was also observed for LVSI prediction (+0.074,  $P=0.018$ ), DMI prediction (+0.088,  $P=0.003$ ), and FIGO stage prediction (+0.066,  $P=0.039$ ) in the validation cohort.

## Discussion

Six prognostic radiomics models of various ROI delineation strategies were constructed in this study, all of which yielded favorable diagnostic performance, demonstrating the potential as non-invasive tools for the prediction of LVSI, DMI, and FIGO stage to guide the management of EC. Our study further found comparable results between

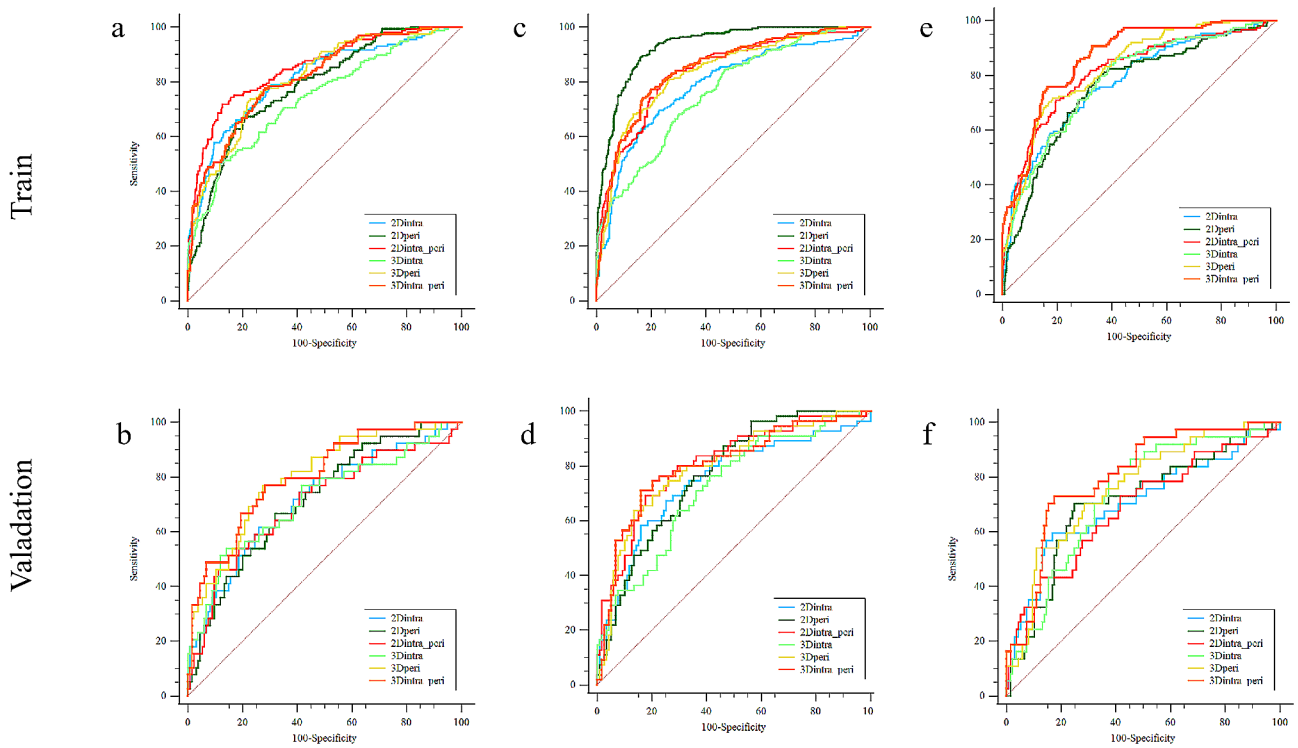


**Fig. 4** The receiver operating characteristic curve analysis results for (a, b) LVSI prediction, (c, d) DMI prediction, and (e, f) disease stage prediction

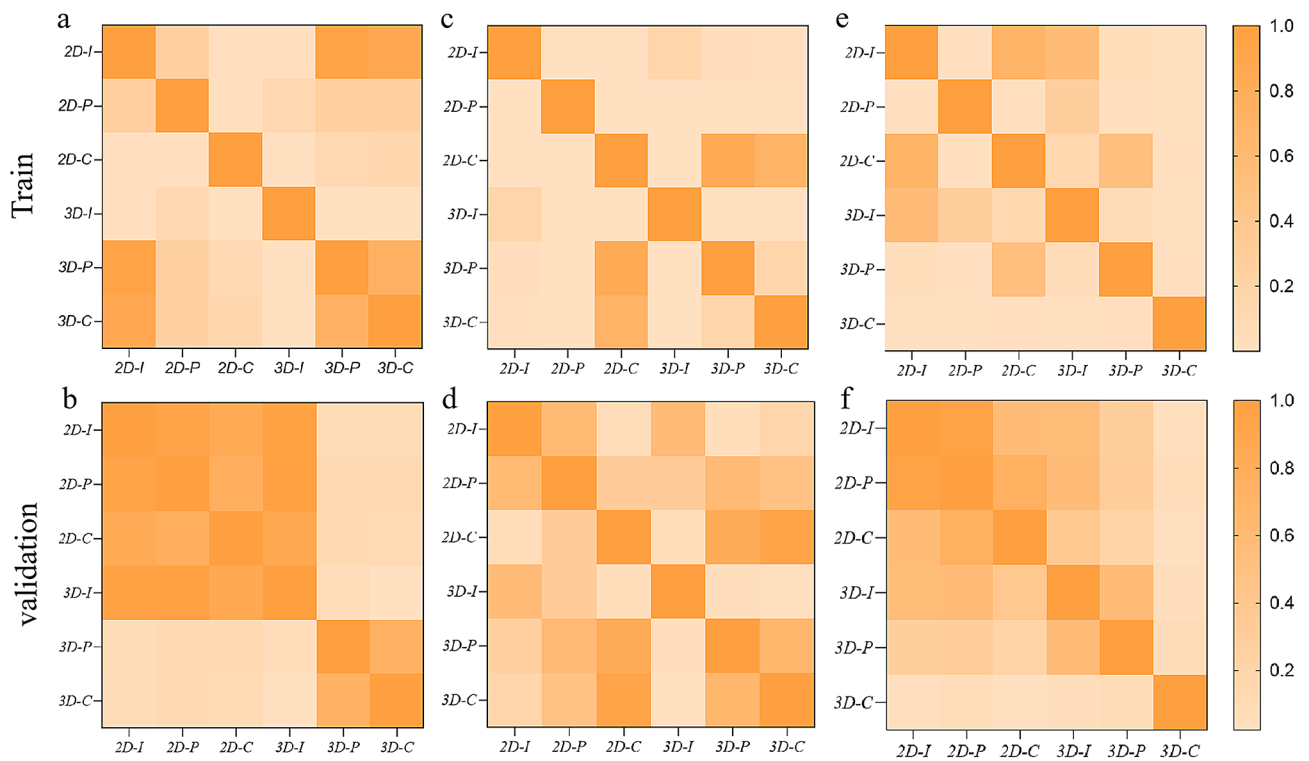


**Fig. 5** The Delong test results for (a, b) LVSI prediction, (c, d) DMI prediction, and (e, f) disease stage prediction between the training and validation cohorts, respectively

the 2D and 3D radiomics models, implying the lack of added value with the more labor-intensive 3D delineation approach. Our findings also demonstrated that assessment of combined intra- and peritumoral features can further enhance the predictive ability of the model.

There has been ongoing debate regarding the use of 2D and 3D radiomics features. Several studies have reported the superiority of 3D models in capturing tumor characteristics, Ortiz-Ramón et al. employed 2D and 3D MRI radiomics to differentiate the origins of brain metastases. Machado et al. utilized MRI radiomics to predict recurrence in clinically non-functioning pituitary macroadenomas. Watzenboeck et al. employed MRI radiomics to assess fetal lung development [27–29], but are often limited in sample size and in their overlooking of peritumoral regions for feature extraction. Our study found comparable performance between 2D and 3D approaches both for intra- and peritumoral ROIs, which is in line with the those of the study by Zhang et al. for tumor phenotype prediction in non-small cell lung carcinomas [30], and the study by Arefan et al. for axillary lymph node metastasis risk in breast cancer [31], which also reported similar performance between 2D and 3D radiomics approaches. However, it's important to note that findings in EC have been mixed. Fasmer et al. [25], using a relatively small sample size, found that 3D whole-tumor radiomic signatures yielded comparable AUC in the training set but significantly lower AUC in the validation set for advanced FIGO stage prediction in EC. These varying results across studies highlight the need for further investigation into the optimal radiomics approach for EC, particularly with larger sample sizes and robust validation.

Such observations may be attributable to the inevitable amplification of noise as the whole tumor volume is delineated across multiple image slices. While 2D ROI delineation within a representative slicing plane may encapsulate key characteristics of the entire tumor volume. Our study highlighted that despite the potential for additional information provided in assessing the entire tumor volume, the marginal gains in predictive ability may not outweigh the practical demands associated with manual multi-slice annotation. This observation could provide support for the promising model performance reported in previous literature, where the utilization of a single slice yielded comparable results [28]. Nonetheless, large-sample studies are warranted for verification of our results.

The growing recognition of the role of the tumor microenvironment in cancer biology has resulted in the recent shift in focus from the primary tumor itself to the surrounding stroma for radiomics feature extraction [32, 33]. Such significance in prognostic value of surrounding tissues has been demonstrated in breast [34] and ovarian

cancers [35]. In this study, we simultaneously developed predictive models through an automated 3 mm boundary expansion of the intratumoral ROI, aimed at capturing spatial characteristics beyond the primary tumor. To our knowledge, this is the first study to compare the effects of 2D versus 3D ROI delineation approaches on peritumoral region. Our results demonstrated useful information that combined models can indeed be attained by inclusion of peritumoral lesion, showed highest diagnostic performance in both the 2D and 3D models, especially 3D models. The obtained AUC results demonstrate reasonable performance and are consistent with those of the study by Yan et al., who demonstrated the complementary nature of intra- and peritumoral features for LVSI and DMI prediction with AUCs of 0.859 and 0.856 respectively [22, 23]. This indicates that, compared to intratumoral features alone, peritumoral regions provide supplementary prognostic information. When coupled with intratumoral radiomics, this minimally invasive multi-regional segmentation provided a balanced assessment of the local tumor-stroma interplay for improved prognostic modeling.

Interesting, the  $3D_{\text{peri}}$  model was observed to significantly outperform the  $3D_{\text{intra}}$  model in our study. This may suggest that tissues in direct contact with the tumor are likely to undergo microstructural alterations prior to histologic changes. 3D peritumoral radiomics may thus offer the sensitivity required for identifying such pre-invasive alterations, and enable a more comprehensive characterization of spatial heterogeneity in the tumor microenvironment. Based on our findings, we propose the potential clinical utility of sampling adjacent stromal tissues, in addition to the primary lesion, for the histopathological assessment of ECs.

Our study had several limitations. First, the retrospective design and relatively modest sample size may limit the generalizability of our findings. Larger prospective studies are thereby needed to validate our results. Second, only a narrow set of histopathological variables with unbalanced cohorts were included due to data availability constraints, these differences could influence the radiomics features extracted and potentially impact the performance of our models. While our study was predominantly endometrioid adenocarcinoma, the validation results demonstrated good stability across the iterations of cross-validation. This suggests that despite pathology variability not fully accounted for, the validation approach helped improve generalizability to these cases Third, the optimal extent of peritumoral expansion was not explored in this study. Fourth, manual delineation may have inevitably resulted in inter-observer variability, which could have been mitigated by utilization of a semi-automated or automated approach. Lastly, more advanced hyperparameter optimization and deep



learning methods were not applied due to the sample size of this study.

## Conclusions

This study developed and investigated the role of 2D and 3D intratumoral and peritumoral radiomics models in the prediction of LVSI, DMI, and disease stage in EC. A 3D ROI delineation approach did not achieve significant improvement in prediction performance. Inclusion of peritumoral features significantly enhanced prediction accuracy of the models, especially the 3D model. Further studies with standardized delineation strategies are warranted to validate our results and advance the clinical translation of radiomics in the field of gynecological oncology.

## Abbreviations

EC	Endometrial cancer
FIGO	International Federation of Gynecology and Obstetrics
LVSI	Lymphovascular space invasion
DMI	Depth of myometrial invasion
MRI	Magnetic resonance imaging
3D	Three-dimensional
2D	Two-dimensional
GLCM	Gray level co-occurrence matrix
GLRLM	Gray level run length matrix
GLSZM	Gray level size zone matrix
NGTDM	Gray tone difference matrix
GLDM	Gray level dependence matrix
LASSO	Least absolute shrinkage and selection operator regression
ROC	Receiver operating characteristic
AUC	Areas under the ROC curve
2D <sub>intra</sub>	Two-dimensional intratumoral model
2D <sub>peri</sub>	Two-dimensional peritumoral model
2D <sub>intra+peri</sub>	Two-dimensional intratumoral + peritumoral model
3D <sub>intra</sub>	Three-dimensional intratumoral model
3D <sub>peri</sub>	Three-dimensional peritumoral model
3D <sub>intra+peri</sub>	Three-dimensional intratumoral + peritumoral model

## Supplementary Information

The online version contains supplementary material available at <https://doi.org/10.1186/s40644-024-00743-2>.

Supplementary Material 1

## Acknowledgements

We would like to thank the native English-speaking scientists of Elixigen Company (Huntington Beach, CA, USA) for editing our manuscript.

## Author contributions

All authors have had access to the data and all drafts of the manuscript. Specific contributions are as follows: design and supervision: RY, XX, NL; development of methodology: SQ, RY; collection and extraction of data: JX, RY, WZ, KL; analysis and interpretation of data (e.g., statistical analysis, algorithm and software development): SQ, RY, PJ; manuscript writing: NL, RY; final approval of manuscript: all authors.

## Funding

This study has received funding by National Natural Science Foundation of China (grant number 81971578, 81701648), the Proof of Concept Program of Zhongguancun Science City and Peking University Third Hospital (grant number HDCXZHKC2022202) and Beijing Natural Science Foundation (grant number Z190020).

## Data availability

The datasets used or analysed during the current study are available from the corresponding author on reasonable request.

## Declarations

### Ethics approval and consent to participate

Institutional Review Board approval was obtained.

### Consent for publication

Written informed consent was obtained from the patient for publication of this research and any accompanying images.

### Competing interests

The authors of this manuscript declare no relationships with any companies, whose products or services may be related to the subject matter of the article.

Received: 26 December 2023 / Accepted: 24 July 2024

Published online: 31 July 2024

## References

- Maheshwari E, Nougaret S, Stein EB, Rauch GM, Hwang K-P, Stafford RJ, et al. Update on MRI in evaluation and treatment of Endometrial Cancer. *Radiographics*. 2022;42:2112–30.
- Feng J, Lin R, Li H, Wang J, He H. Global and regional trends in the incidence and mortality burden of endometrial cancer, 1990–2019: updated results from the global burden of Disease Study, 2019. *Chin Med J*. 2019;137(3):294–302.
- Crosbie EJ, Kitson SJ, McAlpine JN, Mukhopadhyay A, Powell ME, Singh N. Endometrial cancer. *Lancet*. 2022;399:1412–28.
- Siegel RL, Miller KD, Wagle NS, Jemal A. Cancer statistics, 2023. *CA Cancer J Clin*. 2023;73:17–48.
- Peters EEM, Bartosch C, McCluggage WG, Genestie C, Lax SF, Nout R, et al. Reproducibility of lymphovascular space invasion (LVSI) assessment in endometrial cancer. *Histopathology*. 2019;75:128–36.
- Ueno Y, Forghani B, Forghani R, Dohan A, Zeng XZ, Chamming's F, et al. Endometrial carcinoma: MR imaging-based texture model for preoperative risk Stratification—A preliminary analysis. *Radiology*. 2017;284:748–57.
- Zhu X, Ying J, Yang H, Fu L, Li B, Jiang B. Detection of deep myometrial invasion in endometrial cancer MR imaging based on multi-feature fusion and probabilistic support vector machine ensemble. *Comput Biol Med*. 2021;134:104487.
- Colombo N, Creutzberg C, Amant F, Bosse T, González-Martín A, Ledermann J, et al. ESMO-ESGO-ESTRO Consensus Conference on Endometrial Cancer: diagnosis, treatment and follow-up. *Ann Oncol*. 2016;27:16–41.
- Guo W, Wang T, Lv B, Jiang J, Liu Y, Zhao P. Advances in Radiomics Research for Endometrial Cancer: a Comprehensive Review. *J Cancer*. 2023;14:3523–31.
- Arnaiz J, Muñoz A-B, Verna V, Gonzalez-Rodilla I, Schneider J. Magnetic resonance imaging for the Pre-surgical Assessment of Endometrial Cancer: results in a Routine Clinical setting, outside dedicated trials; a cross-sectional study. *Anticancer Res*. 2016;36:1891–4.
- Lambin P, Leijenaar RTH, Deist TM, Peerlings J, de Jong EEC, van Timmeren J, et al. Radiomics: the bridge between medical imaging and personalized medicine. *Nat Rev Clin Oncol*. 2017;14:749–62.
- Bitencourt AGV, Gibbs P, Rossi Saccarelli C, Daimiel I, Lo Gullo R, Fox MJ, et al. MRI-based machine learning radiomics can predict HER2 expression level and pathologic response after neoadjuvant therapy in HER2 overexpressing breast cancer. *EBioMedicine*. 2020;61:103042.
- Yu J, Shi Z, Lian Y, Li Z, Liu T, Gao Y, et al. Noninvasive IDH1 mutation estimation based on a quantitative radiomics approach for grade II glioma. *Eur Radiol*. 2017;27:3509–22.
- Jiang X, Song J, Zhang A, Cheng W, Duan S, Liu X, et al. Preoperative Assessment of MRI-Invisible Early-Stage Endometrial Cancer with MRI-Based Radiomics Analysis. *J Magn Reson Imaging*. 2023;58:247–55.
- Huang Y-Q, Liang C-H, He L, Tian J, Liang C-S, Chen X, et al. Development and validation of a Radiomics Nomogram for Preoperative Prediction of Lymph Node Metastasis in Colorectal Cancer. *J Clin Oncol*. 2016;34:2157–64.
- Bereby-Kahane M, Dautry R, Matzner-Lober E, Cornelis F, Sebbag-Sfez D, Place V, et al. Prediction of tumor grade and lymphovascular space invasion

- in endometrial adenocarcinoma with MR imaging-based radiomic analysis. *Diagn Interv Imaging*. 2020;101:401–11.
17. Stanzone A, Cuocolo R, Del Grosso R, Nardiello A, Romeo V, Travaglino A, et al. Deep myometrial infiltration of Endometrial Cancer on MRI: a Radiomics-Powered Machine Learning Pilot Study. *Acad Radiol*. 2021;28:737–44.
  18. Bc Y, Y L, Fh M, Gf Z, F F, Mh S, et al. Radiologists with MRI-based radiomics aids to predict the pelvic lymph node metastasis in endometrial cancer: a multicenter study. *Eur Radiol*. 2021;31(1):411–22.
  19. Veeraraghavan H, Friedman CF, DeLair DF, Ninčević J, Himoto Y, Bruni SG, et al. Machine learning-based prediction of microsatellite instability and high tumor mutation burden from contrast-enhanced computed tomography in endometrial cancers. *Sci Rep*. 2020;10:17769.
  20. Yan BC, Li Y, Ma FH, Feng F, Sun MH, Lin GW, et al. Preoperative Assessment for High-Risk Endometrial Cancer by developing an MRI - and clinical-based Radiomics Nomogram: a Multicenter Study. *Magn Reson Imaging*. 2020;52:1872–82.
  21. Zhao M, Wen F, Shi J, Song J, Zhao J, Song Q, et al. MRI-based radiomics nomogram for the preoperative prediction of deep myometrial invasion of FIGO stage I endometrial carcinoma. *Med Phys*. 2022;49:6505–16.
  22. Yan B, Zhao T, Li Z, Ren J, Zhang Y. An MR-based radiomics nomogram including information from the peritumoral region to predict deep myometrial invasion in stage I endometrioid adenocarcinoma: a preliminary study. *BJR*. 2023;96:20230026.
  23. Yan B, Jia Y, Li Z, Ding C, Lu J, Liu J, et al. Preoperative prediction of lymphovascular space invasion in endometrioid adenocarcinoma: an MRI-based radiomics nomogram with consideration of the peritumoral region. *Acta Radiol*. 2023;64:2636–45.
  24. Lin Z, Wang T, Li Q, Bi Q, Wang Y, Luo Y, et al. Development and validation of MRI-based radiomics model to predict recurrence risk in patients with endometrial cancer: a multicenter study. *Eur Radiol*. 2023;33:5814–24.
  25. Fasmer KE, Hodneland E, Dybvik JA, Wagner-Larsen K, Trovik J, Salvesen Ø, et al. Whole-volume Tumor MRI Radiomics for Prognostic modeling in Endometrial Cancer. *J Magn Reson Imaging*. 2021;53:928–37.
  26. The image biomarker standardisation initiative. — IBSI 0.0.1 dev documentation. <https://ibsi.readthedocs.io/en/latest/#>
  27. Ortiz-Ramon R, Larroza A, Arana E, Moratal D. A radiomics evaluation of 2D and 3D MRI texture features to classify brain metastases from lung cancer and melanoma. *Annu Int Conf IEEE Eng Med Biol Soc*. 2017;2017:493–6.
  28. Machado LF, Elias PCL, Moreira AC, Dos Santos AC, Murta Junior LO. MRI radiomics for the prediction of recurrence in patients with clinically non-functioning pituitary macroadenomas. *Comput Biol Med*. 2020;124:103966.
  29. Watzenboeck ML, Heidinger BH, Rainer J, Schmidbauer V, Ulm B, Rubesova E, et al. Reproducibility of 2D versus 3D radiomics for quantitative assessment of fetal lung development: a retrospective fetal MRI study. *Insights Imaging*. 2023;14:31.
  30. Zhang X, Zhang G, Qiu X, Yin J, Tan W, Yin X, et al. Radiomics under 2D regions, 3D regions, and peritumoral regions reveal tumor heterogeneity in non-small cell lung cancer: a multicenter study. *Radiol med*. 2023;128:1079–92.
  31. Arefan D, Chai R, Sun M, Zuley ML, Wu S. Machine learning prediction of axillary lymph node metastasis in breast cancer: 2D versus 3D radiomic features. *Med Phys*. 2020;47:6334–42.
  32. P K, A O. Hallmarks of cancer: interactions with the tumor stroma. *Exp Cell Res*. 2010;316(8):1324–31.
  33. Li R. Peritumoral Radiomics and Predicting Treatment Response. *JAMA Netw Open*. 2020;3:e2016125.
  34. Xu H, Liu J, Chen Z, Wang C, Liu Y, Wang M, et al. Intratumoral and peritumoral radiomics based on dynamic contrast-enhanced MRI for preoperative prediction of intraductal component in invasive breast cancer. *Eur Radiol*. 2022;32:4845–56.
  35. Wu Y, Jiang W, Fu L, Ren M, Ai H, Wang X. Intra- and peritumoral radiomics for predicting early recurrence in patients with high-grade serous ovarian cancer. *Abdom Radiol*. 2022;48:733–43.

#### Publisher's Note

Springer Nature remains neutral with regard to jurisdictional claims in published maps and institutional affiliations.